

# Cost Estimation for Green Hydrogen Production and Distribution

Evangelos Chatzistylianos\*, Georgios Psarros, Periklis Chinaris, Stavros Papanthassiou  
Department of Electrical & Computer Engineering, National Technical University of Athens  
Athens, Greece  
\*vxatzistylianos@mail.ntua.gr

**Abstract**—This study addresses the need for a comprehensive assessment of the levelized cost of hydrogen (LCOH) by evaluating green hydrogen production and transportation across the entire hydrogen supply chain. A linear programming (LP) optimization algorithm is employed to determine the optimal siting and sizing of electrolyzers (ELZs) powered by solar or wind energy, with potential integration of battery energy storage systems (BESS) to further improve renewable energy utilization. Results show that optimal ELZ capacities range from 10% to 20% of the RES plant capacity, yielding LCOH between €4.8 and €4.9/kg. Optimal configuration includes wind farms and the ELZ located closer to the consumption-site. However, the analysis reveals that green hydrogen remains less competitive compared to grey and blue alternatives, emphasizing the need for further cost reductions and efficiency improvements to enhance the economic viability of green hydrogen.

**Index Terms**—green hydrogen, LCOH, renewable energy

## I. INTRODUCTION

As energy systems transition towards near-zero emission solutions, hydrogen ( $H_2$ ) emerges as a key enabler for achieving deep decarbonization of the energy sector [1]. It integrates into both the gas and electricity sectors [2], making it a key fuel for a sustainable future. Currently, the predominant method for hydrogen production is steam methane reforming (SMR), [3], converting natural gas into  $H_2$  – commonly referred to as grey hydrogen – while emitting significant amounts of carbon dioxide ( $CO_2$ ). Another method uses coal (or lignite) as a feedstock to produce black (or brown) hydrogen, resulting in even higher  $CO_2$  emissions. If the  $CO_2$  emissions from these processes are mitigated using carbon capture and storage (CCS) technologies, the resulting  $H_2$  is termed blue hydrogen, [4]. In contrast, green  $H_2$  is produced exclusively using renewable energy sources and does not generate any carbon emissions during its production process [5]. Consequently, green hydrogen has gained significant research interest, examining various renewable energy sources (RES) and types of electrolyzer (ELZ).

Recent studies primarily focus on solar- or wind- driven ELZs [6], while less common renewable technologies, like geothermal [7], concentrated solar power (CSP) [8], and run-of-river hydropower plants [9], have received comparatively

limited attention. Additionally, many researchers examine using the electrical grid for  $H_2$  production, but this may include non-renewable energy sources, resulting in hydrogen that is not entirely “green”, [10].

Beyond the choice of energy source, various hydrogen production methods have also been explored. For example, proton-exchange-membrane (PEM), alkaline (ALK) and high temperature electrolysis (THE) have been employed in [11] to produce green  $H_2$  using surplus wind energy. Similarly, solid oxide electrolysis combined with solar energy is utilized in [12] to meet daily  $H_2$  production targets. Among these, PEM and ALK systems are the most extensively researched and technologically mature options, [13], [14].

In addition to the technology employed in hydrogen production process, the siting of the energy source and the electrolyzer is another critical aspect under optimization. One possible configuration involves co-locating the RES plant and the ELZ, allowing direct energy supply to the ELZ. This approach necessitates further examination upon the transportation of produced hydrogen [1].

Alternatively, some studies propose establishing a power purchase agreement (PPA) between a green energy producer and the electrolyzer. In this case, energy is supplied indirectly via the electrical grid, exploiting its transfer capabilities, resulting in an on-grid electrolytic hydrogen system [15]. While this method eliminates the need for hydrogen transport to the end consumer, it incurs auxiliary costs due to the use of national grid infrastructure.

Although numerous studies have explored the production of green hydrogen, a comprehensive cost assessment encompassing the entire hydrogen value chain – from production to end-user delivery – remains essential. This paper addresses the gap by estimating the levelized cost of hydrogen (LCOH), factoring in green hydrogen production, transportation costs, and shedding light into the optimal capacity and location of ELZs. The analysis considers the proximity of ELZs to either RES plant or consumption sites, examining hydrogen transportation in the first case as either compressed gaseous hydrogen ( $CGH_2$ ) or liquified hydrogen ( $LH_2$ ). Solar and wind energy are the renewable sources investigated, paired with PEM electrolyzers.

Using a linear programming (LP) optimization algorithm, the study evaluates the optimal siting and sizing of ELZs, while it also investigates potential BESS integration to enhance performance and cost-effectiveness of produced hydrogen. Finally, a financial comparison is conducted between green hydrogen and its grey and blue alternatives, analyzing how the LCOH differs across these options and assessing the competitiveness of green  $H_2$ .

The remainder of this paper is structured as follows: Section II outlines the formulation of the optimization algorithm. Section III delves into the details of the case study examined, while Section IV focuses on the estimation of the LCOH across various siting and sizing configurations. Finally, Section V summarizes the key findings of the study.

## II. METHODOLOGY

### A. Hydrogen Supply Chain

A holistic overview of the hydrogen supply chain is depicted in Figure 1, outlining two cases: scenario A, where the ELZ is near the RES plant and scenario B, where the ELZ is near the consumption site. Both scenarios include hydrogen production and storage processes, with hydrogen delivered at high-pressures (e.g. 200 bars) [16]. Electrolysis of deionized water drives production, while low-pressure hydrogen storage serves as a buffer between hydrogen production and transportation or distribution. This buffer addresses the variability of renewable energy sources and prevents energy spillage caused by ELZ sizing constraints that might otherwise reduce hydrogen production. Storage capacity is optimized for each ELZ-BESS configuration, ensuring sufficient capacity to handle a single day's maximum hydrogen production.

In scenario A electrolysis energy is directly supplied to the ELZ at the levelized cost of energy (LCOE) of the RES plant. Hydrogen is transported as either  $CGH_2$  or  $LH_2$ , as shown in scenario A of Figure 1. Since both achieve high energy densities, transportation does not occur at low-pressures, For  $CGH_2$ , hydrogen is compressed to 200 bars, necessitating a compression unit sized for peak hourly production.  $LH_2$  requires a liquefier unit to convert gaseous hydrogen into liquid form, also designed for peak capacity. At the end-user site,  $LH_2$  undergoes gasification and is compressed to 200 bars for final delivery.

Transportation costs for both  $CGH_2$  and  $LH_2$  are based on truck delivery. Due to its higher energy density,  $LH_2$  allows for larger hydrogen transport per trip than  $CGH_2$ . The number of trucks required is calculated to ensure continuous operation, with at least one truck always available for loading hydrogen. Total transportation costs for each configuration include fixed costs associated with the number of trucks and variable costs, such as fuel expenses, determined by fuel cost per route and the total number of routes required to deliver to end-users.

In scenario B, the energy required for electrolysis is sourced from the grid at a fixed price set by a power purchase agreement (PPA) between the ELZ and the renewable supplier. The PPA strike price is assumed to align with the LCOE of the RES plant. Nevertheless, additional costs are incurred in this case due to the reliance on the national grid. These expenses include system usage charges and grid access

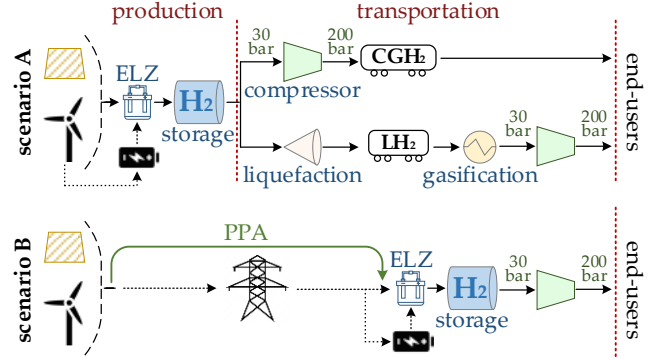


Figure 1: Examined scenarios schematic explanation

fees, which are typically determined based on the consumer's peak or total demand. Moreover, an investment in an HV substation is required for the ELZ in this scenario.

### B. Optimization Algorithm for Hydrogen Generation

The optimization algorithm, employed in this study, is defined by equations (1) to (12), modeling technical and operational constraints of hydrogen generation, while maximizing hydrogen production. The algorithm is designed to maximize total hydrogen generation and is applied consistently across different configurations, irrespective of ELZ proximity to the energy source or the transportation scenario under consideration.

To achieve minimum LCOH for any given configuration, maximizing hydrogen production is imperative. Accordingly, as described in constraint (1), the objective function of the algorithm is structured to maximize the output of the ELZ. This output ( $ELZ_{output}^t$ ) represents the hydrogen produced in terms of energy, measured in megawatt-hours (MWh).

Furthermore, the station equilibrium is described in (2), where energy from RES ( $P_{RES}^t$ ) and BESS discharging ( $P_{dis}^t$ ) equals the energy drawn by the ELZ ( $P_{ELZ}^t$ ) and BESS charging ( $P_{ch}^t$ ). Constraint (3) limits energy supply from RES based on available RES energy ( $A_{RES,t}$ ) and the installed RES capacity ( $I_{RES}$ ), while constraints (4) and (5) limit BESS charge and discharge based on the installed BESS power capacity ( $I_{BESS}^{power}$ ), also accounting for the binary variable ( $o_{BESS}^t$ ) to prevent simultaneous charging and discharging. Similarly, energy drawn from the electrolyzer is limited by the installed ELZ capacity ( $I_{ELZ}$ ) in constraint (6). Finally, constraint (7) describes the BESS state-of-charge ( $SoC_{BESS}^t$ ), considering efficiency of charge-discharge procedure, and constraint (8) limits the energy stored within the battery by its energy capacity ( $I_{BESS}^{energy}$ ).

$$\text{obj: } \max \{ \sum_t ELZ_{output}^t \} \quad (1)$$

$$P_{RES}^t + P_{dis}^t = P_{ELZ}^t + P_{ch}^t \quad \forall t \quad (2)$$

$$P_{RES}^t \leq A_{RES,t} \cdot I_{RES} \quad \forall t \quad (3)$$

$$P_{dis}^t \leq I_{BESS}^{power} \cdot o_{BESS}^t \quad \forall t \quad (4)$$

$$P_{ch}^t \leq I_{BESS}^{power} \cdot (1 - o_{BESS}^t) \quad \forall t \quad (5)$$

$$P_{ELZ}^t \leq I_{ELZ} \quad \forall t \quad (6)$$

$$SoC_{BESS}^t = SoC_{BESS}^{t-1} + P_{ch}^t \cdot \eta_{BESS} - P_{dis}^t / \eta_{BESS} \quad \forall t \quad (7)$$

$$\text{SoC}_{\text{BESS}}^t \leq I_{\text{BESS}}^{\text{energy}} \forall t \quad (8)$$

The ELZ input-output relationship is non-linear due to the non-linear efficiency curve of the water electrolysis process. To address this, a linear approximation of the non-linear efficiency is used, following the principles outlined in [17]. This approach enables the model to accurately reflect ELZ's efficiency using equations (9) to (12). The non-linear relationship, shown as the red line in Figure 2, is approximated by linear segments (dashed black lines in the same figure). A binary variable ( $v_{b,t}$ ) is introduced to activate the block corresponding to the ELZ input power range, with constraint (9) ensuring that only one block is active at a time.

Additionally, an auxiliary variable ( $\text{aux}_{b,t}$ ) is constrained within the minimum ( $\underline{\text{BL}}_b$ ) and maximum ( $\overline{\text{BL}}_b$ ) values of active block, defined in constraint (10). Constraint (11) equates the auxiliary variable to the ELZ input power. Finally, constraint (12) reproduces the standard linear equation, incorporating the minimum y-value of the active block ( $\underline{Y}_b$ ), the slope of the corresponding segment ( $\lambda_b$ ), and the actual input power.

$$\sum_b v_{b,t} = 1 \forall t \quad (9)$$

$$\underline{\text{BL}}_b \cdot v_{b,t} \leq \text{aux}_{b,t} \leq \overline{\text{BL}}_b \cdot v_{b,t} \forall t \quad (10)$$

$$\sum_b \text{aux}_{b,t} = P_{\text{ELZ}}^t \quad (11)$$

$$\text{ELZ}_{\text{output}}^t = \sum_b \{ \underline{Y}_b \cdot v_{b,t} + \lambda_b \cdot (\text{aux}_{b,t} - \underline{\text{BL}}_b \cdot v_{b,t}) \} \quad (12)$$

### C. Financial Assessment

The described algorithm determines the maximum hydrogen production for each ELZ and BESS configuration. In scenario A, hydrogen must be transported to end-users, incurring additional costs that increase the overall hydrogen cost. Conversely, in scenario B, hydrogen is produced on-site; however, the energy drawn from the grid is more expensive than the direct utilization of renewable energy in scenario A.

The levelized cost of hydrogen (LCOH) is the key metric for comparing scenarios with varying capital costs and hydrogen production outputs. It represents the price at which hydrogen must be sold to achieve the target internal rate of return (IRR) and is calculated using equation (13). The LCOH accounts for several components: the total initial investment for all assets (CAPEX), including the electrolyzer and the battery investment, the annual operational and maintenance costs associated with maintaining these assets (O&M), the cost of electricity ( $C_y^E$ ) and water ( $C_y^W$ ) used in the electrolysis process, inflation ( $ir$ ), the tax rate ( $tr$ ) and asset depreciation ( $D_y$ ). Scenario-specific costs, such as transportation expenses and grid fees, are further incorporated in the formula to assess the overall LCOH of each scenario examined.

Finally, the total hydrogen produced ( $H_2^y$ ) serves as the denominator, ensuring expenses are proportionally allocated per unit of hydrogen produced. This comprehensive approach enables an accurate evaluation of the cost-efficiency and economic viability of hydrogen production across different scenarios

$$\text{LCOH} = \frac{\text{CAPEX} + \sum_y [(O\&M_y \cdot (1+ir)^y + C_y^E + C_y^W) \cdot (1-tr) \cdot D_y \cdot tr] / (1+i)^y}{(1-tr) \cdot \sum_y H_2^y / (1+i)^y} \quad (13)$$

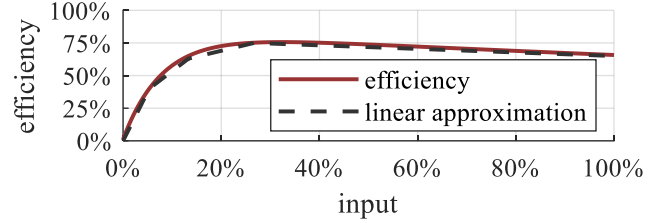


Figure 2: Efficiency (and its linear approximation) of the electrolyzer

The formula for calculating the levelized cost of energy (LCOE), which represents the price of energy consumption, is given in equation (14). Similar to LCOH, it includes the capital expenditures of the RES plant, annual O&M costs and linear depreciation over its useful life. The denominator in the calculation is the total renewable energy produced ( $E_y$ ), irrespective of the amount consumed by the electrolyzer.

$$\text{LCOE} = \frac{\text{CAPEX} + \sum_y [(O\&M_y \cdot (1+ir)^y) \cdot (1-tr) \cdot D_y \cdot tr] / (1+i)^y}{(1-tr) \cdot \sum_y E_y / (1+i)^y} \quad (14)$$

To compare green hydrogen with grey and blue hydrogen, the LCOH for green hydrogen is evaluated alongside the LCOH of hydrogen produced using natural gas (NG). Investment costs for NG-based hydrogen production include the SMR unit and, in the case of blue hydrogen, the carbon capture unit. Additionally, the total expenses for grey and blue hydrogen account for the costs of natural gas and the CO<sub>2</sub> cost with carbon emission price under the Emissions Trading System (ETS) during the production process.

### III. CASE STUDY

This study considers PV plants with an energy yield of 1530 kWh/kW and WFs with a 30.2% capacity factor. The investment costs for PVs and WFs are €500/kW and €1,200/kW, respectively. The ELZ investment cost follows an economies-of-scale approach, starting at €1,000/MW for 1 MW capacity and decreasing to €700/MW for 100 MW. Figure 2 illustrates ELZ efficiency with a 100-step linear approximation. Lastly, in Scenario A, the distance between the production and consumption site is assumed to be 500 km.

The capital cost of hydrogen storage is 200 €/kg of produced hydrogen, while the compressor CAPEX, is calculated based on formulas in [18]. The liquefaction unit costs €36,000/kg/h, and the regasification unit costs €4,500/kg/h. Deionized water is priced at €2.5/m<sup>3</sup>, with 10 liters required to produce 1kg of hydrogen. The project IRR, used in LCOH and LCOE calculations, is assumed to be 7%.

In scenario B, system usage costs include energy and capacity charges. The energy charge is €4/MWh, applied to the total energy consumed, while the capacity charge is €24,000/MW based on installed capacity. Additionally, a cost of €100/kW is allocated for the HV substation.

Battery storage systems consist of power and energy components, with costs of €100/kW and €150/kWh, respectively. The investment lifetime for most assets is 20 years, matching the project timeline. However, the energy component experiences capacity fade due to continuous usage, reducing its lifespan to 10 years, requiring replacement at the end of the 10th year to maintain system performance.

The examined configurations feature a RES plant with a

capacity of 100 MW, paired with ELZs ranging from 2 MW to 100 MW. In scenarios involving BESS, the power capacity of the BESS is set equal to ELZ capacity, while energy capacity is configured for durations of 1-hour, 2-hours, and 4-hours. Finally, the LCOH of grey and blue hydrogen is derived based on cost assumptions from [19].

#### IV. RESULTS

##### A. Scenarios without battery storage systems

Besides the LCOH, which serves as the key metric for comparing various configurations, several other aspects of the hydrogen supply chain should also be examined to provide a more comprehensive understanding of the system. In this context, Figure 3a illustrates the renewable energy consumption by the electrolyzer as a percentage of the total available renewable generation, reflecting the utilization factor of the RES plant. This factor reaches a plateau at higher ELZ capacities, indicating that beyond this point the ELZ is sufficiently large to fully utilize the entire renewable energy production. Additionally, Figure 3b presents the capacity factor of the ELZ. The integration of the more efficient WF leads to nearly double the capacity factor of the ELZ compared to the PV plant. For smaller ELZ capacities, the smoother and more consistent production profile of the WF, in contrast to the concentrated generation pattern of PVs, results in a more significant difference in this metric. Finally, Figure 3c depicts the annual hydrogen production, which follows the trend of the renewable usage rate. As the ELZ capacity increases, the higher efficiency of WFs is further leveraged, resulting in significantly greater hydrogen production compared to PVs.

The production process is consistent across both scenarios. Consequently, the production cost of hydrogen, which includes the ELZ investment and energy and water costs during electrolysis, is similar regardless of transportation or grid connection considerations. As such, Figure 4a and Figure 4b – illustrating the LCOH of the production process for hydrogen sourced from PVs and WFs, respectively- are the same in both scenarios. For PVs, ELZ investment and energy costs are comparable, whereas WFs' higher capacity factor makes energy cost dominant. Water cost remains negligible in both cases. Optimal ELZ capacities are found to be between 10% and 20% of the RES plant capacity, yielding LCOH values between €4.8 and €4.9/kg. Notably, ELZs supplied by WFs achieve LCOH values that are €0.05-€0.40/kg lower than those supplied by PVs, due to the higher cost-effectiveness of wind energy.

The total LCOH includes transportation or additional grid expenses in addition to the production LCOH, reflecting the price hydrogen must be sold at to end-users. Figure 5 presents the total LCOH, with solid lines representing PVs, and dashed lines representing WFs, across the three examined scenarios: a) transportation of hydrogen as CGH<sub>2</sub>, b) transportation of hydrogen as LH<sub>2</sub> and c) scenario B, that considers grid fees.

Although wind energy utilization results in a lower production LCOH, transporting larger volumes of hydrogen as CGH<sub>2</sub> or LH<sub>2</sub> increases the total LCOH when ELZ capacity exceeds 20% due to the significantly higher hydrogen production. Conversely, locating the ELZ near the

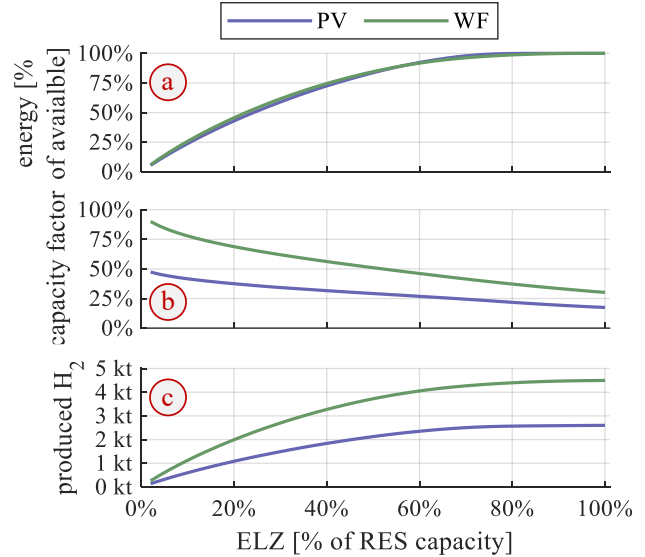


Figure 3: a) Utilized renewable generation, b) capacity factor of ELZ and c) total hydrogen production: for ELZ paired with PV and WF consumption site eliminates the need for transportation, reducing the total LCOH by approximately €0.3/kg on average and making WF more favorable than PVs. Overall, placing the ELZ near the consumption site generally leads to lower total LCOH, reaching €5.6/kg in the optimal configuration, except for large ELZ capacities. In those cases, the high energy demand results in significant grid utilization fees, increasing the total LCOH.

##### B. Scenarios with battery storage systems

The incorporation of BESS significantly boosts hydrogen production, mainly when paired with PV systems. Smaller ELZs enable daily full charging from concentrated solar generation, leading to at least one complete cycle per day. In contrast, the higher and more consistent energy output of wind systems reduces the relative impact of BESS on hydrogen production. Figure 6 presents the total hydrogen produced for both: a) PV supply and b) WF supply. For smaller ELZ capacities, the limited BESS capacity relative to the RES plant results in only a modest increase in hydrogen production. Additionally, the production plateau is reached at lower ELZ capacities when batteries are present, as renewable energy is fully utilized through storage.

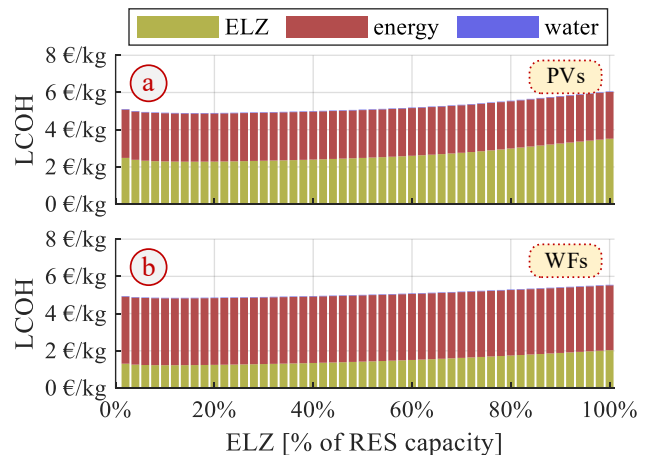


Figure 4: LCOH of hydrogen production for ELZ with a) PV and b) WF

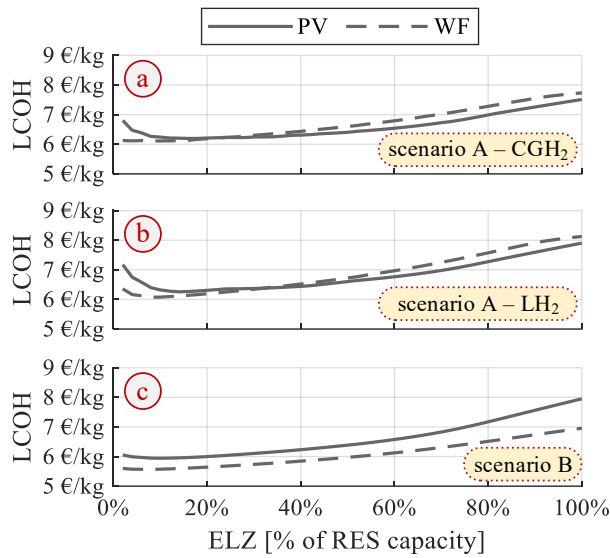


Figure 5: Total LCOH for a) transportation as CGH<sub>2</sub>, b) transportation as LH<sub>2</sub> and c) scenario B: ELZ near consumption-site

However, the additional hydrogen production achieved with the inclusion of BESS is insufficient to offset the increase in total expenses. As a result, total LCOH rises at least €0.5/kg (8%) with BESS, with larger increases for high ELZ capacities where battery effectiveness declines. Figure 7 presents the total LCOH increase across all examined cases in the presence of storage.

### C. Comparison between green and brown/blue hydrogen

Production costs of grey and blue hydrogen vary depending on fuel prices and CO<sub>2</sub> emission rights costs. As shown in Figure 8, the optimal LCOH for green hydrogen from this analysis, represented by the green solid line, remains higher than that of grey or blue hydrogen, except in cases of excessively high costs.

To improve the competitiveness of green hydrogen against fossil-fuel-based production methods, significant reductions in total LCOH. More specifically, a CAPEX reduction of approximately 25%-30% is necessary for green hydrogen to achieve price parity with fossil-fuel-based alternatives.

## V. CONCLUSIONS

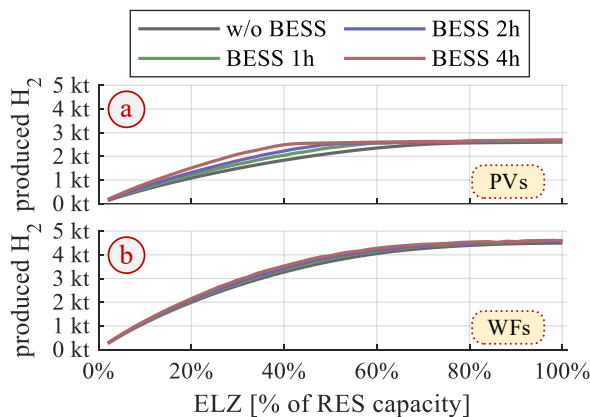


Figure 6: Total produced hydrogen for ELZ paired with a) PV and b) WF

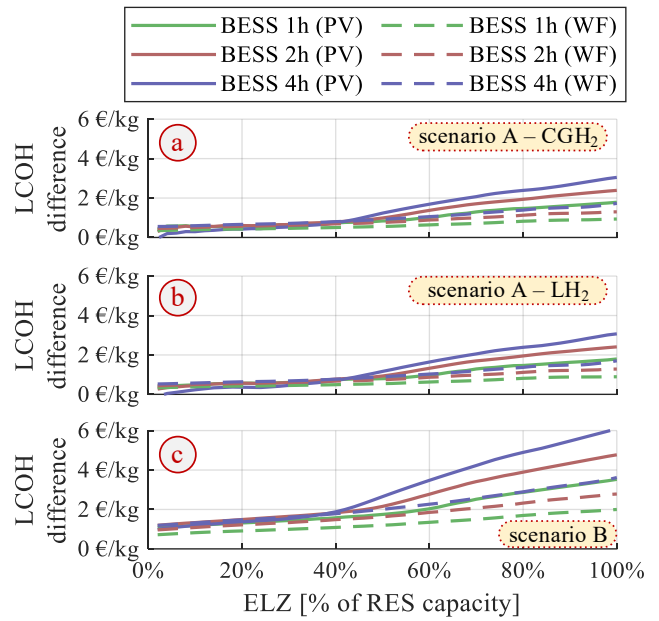


Figure 7: Difference in LCOH in the presence of BESS for: a) transportation as CGH<sub>2</sub>, b) transportation as LH<sub>2</sub>, and c) ELZ near consumption-site

This study explored the techno-economic performance of hydrogen production systems powered by RES, analyzing scenarios with and without BESS. Optimal ELZ capacities (10%-20% of RES) yield lower LCOH with WFs due to higher capacity factors. Locating ELZs near consumption sites reduced the total LCOH by approximately €0.3/kg by eliminating transportation costs, though grid utilization fees became significant for large ELZ capacities.

The incorporation of BESS enhanced hydrogen production, particularly with PV systems, due to their concentrated generation profile, while WFs showed less dependence on storage. However, the increased production was insufficient to offset the higher expenses introduced by BESS, leading to an average rise in total LCOH by €0.5/kg, with larger increases observed at higher ELZ capacities.

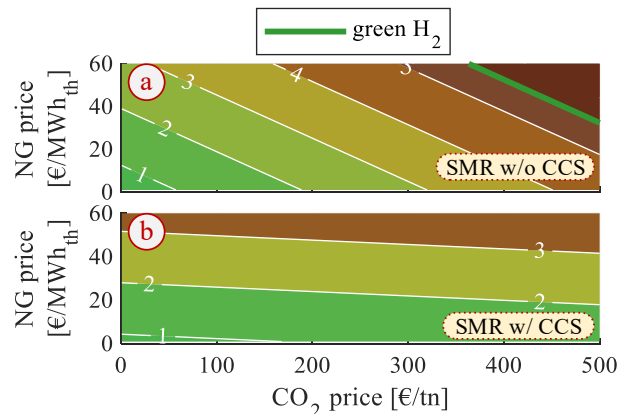


Figure 8: LCOH of green H<sub>2</sub> (green line) against: a) grey and b) blue H<sub>2</sub>

## REFERENCES

- [1] M. Reuß, P. Dimos, A. Léon, T. Grube, M. Robinius, and D. Stolten, "Hydrogen road transport analysis in the energy system: A case study for Germany through 2050," *Energies (Basel)*, vol. 14, no. 11, Jun. 2021, doi: 10.3390/en14113166.
- [2] P. P. Chinaris, G. N. Psarros, E. S. Chatzistylianou, and S. A. Papathanassiou, "Impact of Natural Gas Price Variations and Consumption Limitation on the Decarbonization of Sector-Coupled Energy Systems," *IEEE Access*, vol. 11, pp. 131573–131596, 2023, doi: 10.1109/ACCESS.2023.3334397.
- [3] F. Moreno-Brieva, J. Guimón, and J. C. Salazar-Elena, "From grey to green and from west to east: The geography and innovation trajectories of hydrogen fuel technologies," *Energy Res Soc Sci*, vol. 101, Jul. 2023, doi: 10.1016/j.erss.2023.103146.
- [4] M. S. Al-Khelaiwi, T. A. Al-Masaabi, H. Farag, and S. Rehman, "Evaluation of Green and Blue Hydrogen Production Potential in Saudi Arabia," *Energy Conversion and Management: X*, vol. 24, Oct. 2024, doi: 10.1016/j.ecmx.2024.100742.
- [5] J. L. Fan, P. Yu, K. Li, M. Xu, and X. Zhang, "A levelized cost of hydrogen (LCOH) comparison of coal-to-hydrogen with CCS and water electrolysis powered by renewable energy in China," *Energy*, vol. 242, Mar. 2022, doi: 10.1016/j.energy.2021.123003.
- [6] H. O. S. Tubalinal *et al.*, "Prospects of green hydrogen production in the Philippines from solar photovoltaic and wind resources: A techno-economic analysis for the present and 2030," *Renew Energy*, vol. 235, Nov. 2024, doi: 10.1016/j.renene.2024.121286.
- [7] M. O. Awaleh, A. B. Adan, O. A. Dabar, M. Jalludin, M. M. Ahmed, and I. A. Guirreh, "Economic feasibility of green hydrogen production by water electrolysis using wind and geothermal energy resources in asal-ghoubbet rift (Republic of Djibouti): A comparative evaluation," *Energies (Basel)*, vol. 15, no. 1, Jan. 2022, doi: 10.3390/en15010138.
- [8] M. Al-Mahmodi, O. Ayadi, and A. Al-Halhouli, "Parametric modeling of green hydrogen production in solar PV-CSP hybrid plants: A techno-economic evaluation approach," *Energy*, vol. 313, Dec. 2024, doi: 10.1016/j.energy.2024.133943.
- [9] D. J. Jovan, G. Dolanc, and B. Pregelj, "Cogeneration of green hydrogen in a cascade hydropower plant," *Energy Conversion and Management: X*, vol. 10, Jun. 2021, doi: 10.1016/j.ecmx.2021.100081.
- [10] Z. Wang, "Identifying green hydrogen produced by grid electricity," *Int J Hydrogen Energy*, vol. 81, pp. 654–674, Sep. 2024, doi: 10.1016/j.ijhydene.2024.07.214.
- [11] B. Olateju and A. Kumar, "Hydrogen production from wind energy in Western Canada for upgrading bitumen from oil sands," *Energy*, vol. 36, no. 11, pp. 6326–6339, 2011, doi: 10.1016/j.energy.2011.09.045.
- [12] L. Mastropasqua, I. Pecenati, A. Giostri, and S. Campanari, "Solar hydrogen production: Techno-economic analysis of a parabolic dish-supported high-temperature electrolysis system," *Appl Energy*, vol. 261, Mar. 2020, doi: 10.1016/j.apenergy.2019.114392.
- [13] F. T. Hong *et al.*, "Minimizing renewable hydrogen costs at producer's terminal gate with alkaline electrolyser, proton exchange membrane, and their co-installment: A regional case study in China," *Int J Hydrogen Energy*, vol. 86, pp. 1051–1062, Oct. 2024, doi: 10.1016/j.ijhydene.2024.08.485.
- [14] J. Park, S. Kang, S. Kim, H. S. Cho, and J. H. Lee, "Comparative techno-economic evaluation of alkaline and proton exchange membrane electrolysis for hydrogen production amidst renewable energy source volatility," *Energy Convers Manag*, vol. 325, Feb. 2025, doi: 10.1016/j.enconman.2024.119423.
- [15] X. Li, X. Tang, M. Ma, M. Wang, and C. Xu, "Levelized cost analysis of onshore wind-powered hydrogen production system in China considering landform heterogeneity," *Energy*, vol. 313, Dec. 2024, doi: 10.1016/j.energy.2024.133942.
- [16] M. Haddad and N. Javani, "Dynamic analysis of green hydrogen production integrated with storage tanks: An economical assessment for different demands," *Int J Hydrogen Energy*, Oct. 2024, doi: 10.1016/j.ijhydene.2024.10.024.
- [17] B. Xu, J. Zhao, T. Zheng, E. Litvinov, and D. S. Kirschen, "Factoring the Cycle Aging Cost of Batteries Participating in Electricity Markets," *IEEE Transactions on Power Systems*, vol. 33, no. 2, pp. 2248–2259, Mar. 2018, doi: 10.1109/TPWRS.2017.2733339.
- [18] T. R. Lucas, A. F. Ferreira, R. B. Santos Pereira, and M. Alves, "Hydrogen production from the WindFloat Atlantic offshore wind farm: A techno-economic analysis," *Appl Energy*, vol. 310, Mar. 2022, doi: 10.1016/j.apenergy.2021.118481.
- [19] M. Katebah, M. Al-Rawashdeh, and P. Linke, "Analysis of hydrogen production costs in Steam-Methane Reforming considering integration with electrolysis and CO<sub>2</sub> capture," *Clean Eng Technol*, vol. 10, Oct. 2022, doi: 10.1016/j.clet.2022.100552.